Tuning the Area Percentage of Reactive Surface of TiO_2 by Strain Engineering

Lan Jia, Da-Jun Shu,* and Mu Wang†

National Laboratory of Solid State Microstructures and Department of Physics, Nanjing University, Nanjing 210093, China

(Received 10 May 2012; published 12 October 2012)

Surfaces with high reactivity usually have a low area percentage, which greatly limits the efficiency of surface reactivity. In this Letter we demonstrate a generic way of increasing the percentage of the highly reactive surface by using external strain. Bulk and surface elastic properties of TiO_2 are studied via density functional theory calculations. The equilibrium shape of anatase TiO_2 under applied strain is discussed based on the elastic properties. We find that when 5% compressive strain is applied biaxially along [100] and [010]; directions, the area percentage of the anatase (001) surface can be increased by ~5 times in comparison with the case when no strain is applied. Since the moderate strain does not introduce extrinsic defects into the material, we propose that it is an ideal way to increase the reactivity of titanium dioxide crystallites by applying biaxial compressive external strain along the *a* axis.

DOI: 10.1103/PhysRevLett.109.156104 PACS numbers: 68.35.Md, 68.35.Gy, 68.47.Gh

Surfaces with high reactivity usually have a low area percentage, which greatly limits the efficiency of surface reactivity. For example, titanium dioxide has attracted much attention due to its promising applications in heterogeneous catalysis, solar cells, gas sensors, photocatalysis, cleaning environments, etc., [1–5]. However, the area of the most reactive (001) surface is only 3% of the total surface of anatase TiO_2 in equilibrium [6–8]. It has been well established that the equilibrium shape of a crystal corresponds to the minimal surface energy under the constraint of fixed volume [9]. Therefore, it is possible to increase the percentage of the reactive surface by changing the surface free energies, and in this way the reactivity of the crystallite can be engineered.

For TiO_2, Yang *et al.* reported that by adsorbing fluorine, the relative stability of surfaces can be changed, which results in a large percentage of the highly reactive (001) surface [10]. Since then lots of work has been reported to tune the area ratio of TiO_2 surface by using chemical methods. However, chemical methods involve additional constituents during the growth processes. The influence of the residuals of these constituents on the material properties is not easy to rule out [11,12].

In comparison, physical methods have the advantage of being clean and simple. For example, moderate strain does not introduce extrinsic defects in the materials. It has been proposed that external strain can be used to change the band gap as well as the formation energy of surface oxygen vacancies of TiO_2 [13–16]. It would be of great significance if one could also apply suitable external strain to increase the area percentage of the reactive surface. To achieve this goal, first of all we need to have the knowledge of the surface elastic properties. Besides, surface elastic properties are also important for understanding the size dependent mechanical properties of nanosized crystals [17]. To our knowledge, however, no systematic study has been carried out to explore the surface elastic properties of TiO_2.

In this Letter, bulk and surface elastic properties of TiO_2 are studied via density functional theory calculations. The equilibrium shape of anatase TiO_2 under applied strain is discussed based on the elastic properties. We find that the area percentage of the highly reactive anatase (001) surface increases up to ~5 times when 5% biaxial compressive strain is applied along the *a* axis, compared to the equilibrium shape of the crystallite when no strain is applied. Therefore, we suggest that strain engineering is an ideal way to increase the reactivity of anatase crystallites.

The calculations are based on density functional theory in the PW91 generalized gradient approximation [18], using the Vienna *ab initio* simulation package (VASP) code with projector augmented wave pseudopotentials [19,20]. The structures of the ideal (100), (001), (101), and (110) surfaces of TiO_2 in rutile and anatase are shown in Fig. 1. Note that the exposed anatase (001) surface is characteristic of surface O-Ti-O bonds in parallel, which makes the surface anisotropic, although the [100] and

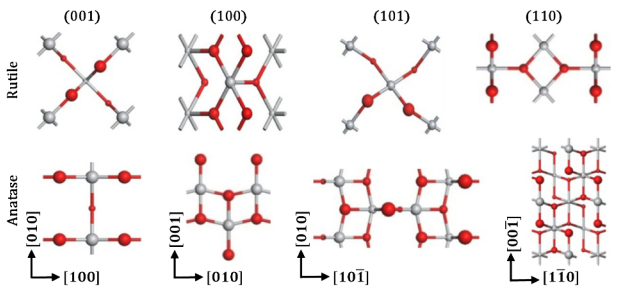

FIG. 1 (color online). Top views of the unrelaxed structures of the rutile and anatase surfaces. Gray and red (dark gray) spheres indicate the titanium and oxygen atoms. The size of the spheres stands for the distance of the atoms from the surfaces schematically. The length scale between different surfaces is not kept.

[010] directions are equivalent in bulk. Each surface is modeled as a (1×1) supercell consisting of a slab and a vacuum with thickness of more than 15 Å. The slab consists of 18 (33), 36 (15), 72 (36), 72 (30) atoms for the (001), (100), (110), (101) surfaces of anatase (rutile), respectively. The Γ-centered Monkhorst-Pack k-point meshes of $7 \times 7 \times 1$ ($5 \times 5 \times 1$), $7 \times 3 \times 1$ ($5 \times 8 \times 1$), $5 \times 3 \times 1$ ($4 \times 8 \times 1$), and $2 \times 7 \times 1$ ($5 \times 5 \times 1$) are used to sample the Brillouin zone of the (001), (100), (110), (101) surfaces of anatase (rutile), respectively. The plane-wave energy cutoff of 500 eV is used for expanding the Kohn-Sham wave functions. All the atoms are relaxed without constraints until the forces are converged to 0.01 eV/Å.

The bulk elastic properties of TiO_2 are described by six independent elastic constants (C_{11}, C_{33}, C_{44}, C_{66}, C_{12}, and C_{13}). Other elastic properties such as the bulk modulus (B) and Young's modulus (Y) can be deduced from the elastic constants. The obtained results are summarized in Table I. We can see that the *soft* direction, i.e., the one most readily to compress, is along the a axis and the c axis for rutile and anatase, respectively. We also show the so-called in-plane Young's modulus Y_r, i.e., the stress-strain ratio when stress is biaxially applied along [100] and [010]. It is slightly smaller than the modulus along the *hard* direction (Y_c) for rutile, but larger than the *hard* modulus (Y_a) for anatase. The values are in good agreement with experimental data [21] and previous theoretical calculations [22,23].

In order to obtain the surface elastic properties, in-plane strain is applied to each surface of anatase and rutile. The Lagrangian surface energy γ_L as a function of the applied strain can be expressed as $\gamma_L(\varepsilon) = (E^{st}(\varepsilon) - E^b(\varepsilon))/2A_L$, where the factor 2 accounts for the two identical surfaces of the symmetrical slab, and A_L is the area of the surface in the unstrained state. $E^{st}(\varepsilon)$ and $E^b(\varepsilon)$ are the total energies of the strained slab and the strained bulk, respectively. Note that the strained energy part of $E^b(\varepsilon)$ cannot be calculated directly from the bulk elastic constants listed in Table I. Instead, one should transform the bulk elastic constants for the coordinate system of each surface in order to account for the condition of the free surface correctly. Denoting the transformation matrix as T, the 4-index elastic constants in the new coordinate system of a surface can be calculated as $C'_{ijkl} = T_{im}T_{jn}T_{ko}T_{lp}C_{mnop}$ according to the definition of elastic constants [24].

TABLE I. The calculated elastic constant C_{ij}, bulk modulus (B), Young's modulus along the a axis (Y_a), along the in-plane r direction (Y_r), and along the c axis (Y_c) of rutile and anatase phases, in units of GPa.

	C_{11}	C_{12}	C_{13}	C_{33}	C_{44}	C_{66}	B	Y_c	Y_r	Y_a
Rutile										
This Letter	265	179	151	472	116	211	209	369	348	138
Exp [21]	268	175	147	484	124	190	212	386	354	147
Phonon [22]	269	189	166	506	105	217	219	386	349	130
PBE [23]	261	132	137	456	117	204	187	360	311	182
Anatase										
This Letter	331	144	141	189	46	59	173	105	264	219
Phonon [22]	333	143	140	198	39	57	176	116	278	226
PBE [23]	311	150	138	191	51	59	172	108	262	199

The surface energies when no strain is applied are from low to high 0.44, 0.70, 1.03, and 1.30 J/m^2 for rutile (110), (100), (101), and (001), respectively. For anatase surfaces, the surface energies are 0.52, 0.59, 1.04, and 1.10 J/m^2 for (101), (100), (001), and (110), respectively. The results are consistent with reported results [7,25]. The surface energies change obviously when in-plane strain is applied, and the extent of the changes depends on the crystallographic orientations both for rutile (not shown) and for anatase as shown in Fig. 2. Here uniaxial strain and biaxial strain ranging from -0.03 to 0.03 are considered, while the nondiagonal components ε_{12} is set to zero since the in-plane shear modulus has little practical significance.

The surface stress tensor $\sigma_{\alpha\beta}$ and surface elastic constants $S_{\alpha\beta\alpha'\beta'}$ are defined as the first and second order derivation of γ_L, respectively [26,27]. Based on the three order polynomial fits displayed with the dashed curves in Fig. 2, the values are obtained as listed in Table II. Among the surfaces, anatase (001) possesses the largest and the most anisotropic surface stress. The surface stress is tensile along the surface bonds ($\sigma_{11} > 0$) and compressive across the bonds ($\sigma_{22} < 0$), consistent with previous reports [28].

The surface elastic constants are negative for the considered surfaces of rutile, and either positive or negative for anatase. This is much different from the case of bulk, where elastic constants are always positive. Considering the fact that a surface cannot exist independently of the

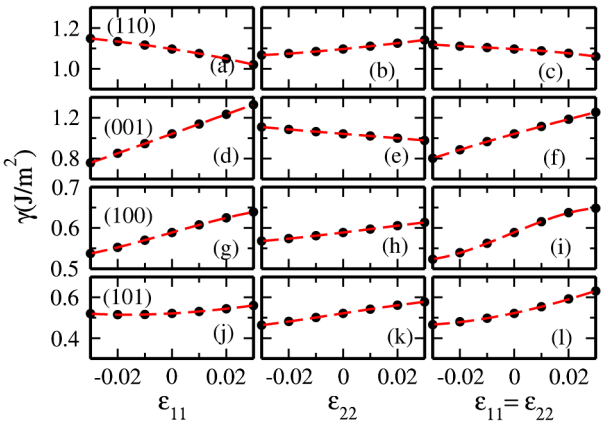

FIG. 2 (color online). Variation of the surface energy of the anatase (101) (a)–(c), (100) (d)–(f), (001) (g)–(i), and (110) (j)–(l) surface with the applied uniaxial (first two columns) and biaxial strain (last column). Dots are calculated results and dashed curves are the three order polynomial fits. Subscripts 11 and 22 denote x and y directions of each surface as displayed in Fig. 1.

TABLE II. The calculated surface energy and surface mechanical properties of rutile and anatase phases. γ, σ, and S denote surface energy, surface stress, and surface elastic constant, respectively. Subscripts 11 and 22 mean the same as in Fig. 2. The units are in J/m^2.

	γ	σ_{11}	σ_{22}	S_{1111}	S_{2222}	S_{1122}
Rutile						
(110)	0.44	2.52	1.14	−73.81	−17.67	−26.30
(100)	0.70	−1.74	1.28	−20.64	−2.88	−9.75
(101)	1.03	−0.08	0.16	−24.62	−25.38	−21.88
(001)	1.30	1.27	1.27	−8.27	−8.27	−15.80
Anatase						
(101)	0.52	0.77	2.06	41.33	−2.21	9.99
(100)	0.59	1.90	0.82	−1.31	4.40	−5.06
(001)	1.04	9.58	−2.13	2.64	2.64	−18.01
(110)	1.10	−2.09	1.31	−27.74	16.07	−2.17

bulk of the material, the negative surface elasticity suggests that the presentation of the corresponding surface makes TiO_2 in nanoscale softer than its bulk phase.

The equilibrium shape can be calculated or graphically obtained by the Wulff construction using the values of surface energies [9]. For anatase it yields a truncated octahedral bipyramid terminated by two equivalent square (001) faces and eight equivalent (101) faces, consistent with the literatures [7,8,10]. Quantitatively, one can write down the area proportion of {101} and {001} surfaces as $\frac{S_{001}}{S_{101}} = \frac{e^2 \cdot \cos\theta}{1-e^2}$, where $e = 1 - (\gamma_{001}/\gamma_{101})\cos\theta$, and θ denotes the angle formed by the (101) and (001) surfaces. The larger the value of e, the larger the area percentage of S_{001}. The obtained area of the reactive (001) surface is ~3% of the total surface area when no strain is applied, which largely limits the efficiency of the surface reactivity of anatase.

For the crystallite under external strain, the in-plane strain condition of the exposed surfaces depends on their respective crystallographic orientations. The strain tensor in the coordinate system of each surface is connected with the one in the bulk system by the transformation matrix of T, $\varepsilon'_{ij} = T_{im}T_{jn}\varepsilon_{mn}$. Here we consider the strain applied to the anatase crystal in three ways, namely, the strain along the c axis while atoms are free along the a axes, the uniaxial strain applied along one of the a axes while fixed along the other a axis and free along the c axis, or the strain biaxially applied along both the [100] and [010] directions while free in the c axis, respectively. For the surfaces considered in this Letter, all the nondiagonal in-plane components of strain are zero. The surface energy of a specific surface of the strained crystal to the second approximation can thus be written as follows,

$$\gamma(\varepsilon) = \gamma_0 + \sigma_{\alpha\alpha}\varepsilon_{\alpha\alpha} + \frac{1}{2}S_{\alpha\alpha\beta\beta}\varepsilon_{\alpha\alpha}\varepsilon_{\beta\beta}, \qquad (1)$$

where α and β denote the two in-plane directions of each surface. The externally applied strain may make the (101) and (011) surfaces inequivalent and reduce the symmetry of anatase to the orthorhombic space group. The formula of the area ratio of the surfaces needs to be generalized accordingly,

$$\frac{S_{001}}{2e_1e_2} = \frac{S_{101}\cos\theta_1}{(1-e_1)(1+e_2)} = \frac{S_{011}\cos\theta_2}{(1+e_1)(1-e_2)}, \qquad (2)$$

where $e_1 = 1 - (\gamma_{001}/\gamma_{101})\cos\theta_1$, and $e_2 = 1 - (\gamma_{001}/\gamma_{011})\cos\theta_2$ with θ_1 (θ_2) being the angle formed by (101) and (001) [(011) and (001)].

As displayed in Fig. 3(a), a dramatic increase of the area percentage of the (001) surface occurs when compressive strain is applied biaxially along the a axes. When the compressive strain is 5%, the area percentage increases by ~5 times compared to the case when no strain is applied. Uniaxial compressive strain along one of the two a axes may either increase or decrease the area percentage of the (001) surface, depending on whether the strain is along or across the surface bonds of the (001) surface [see the inset of Fig. 3(a)]. The real area percentage should be the average of the two cases considering the randomness in the alignment of the surface bonds, as shown by the dashed curve in Fig. 3(a), which is smaller than that under the biaxial strain. The effect of the strain along the c axis is contrary to and less significant than that of the strain along the a axes.

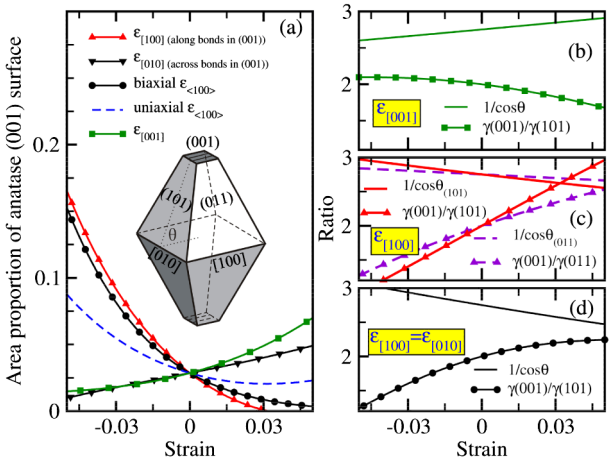

FIG. 3 (color online). (a) The area percentage of anatase (001) facets with variation of the applied strain. External strain is applied uniaxially along the surface bonds in (001) (up triangles), across the bonds (down triangles), biaxially along [100] and [010] (circles), or along the c axis (squares). The dashed curve shows the average of the area percentage when strain is applied along and across the surface bonds of (001) surface separately. The inset displays the equilibrium shape of the anatase crystallite, where the lines along [100] direction of (001) surfaces shows the surface bonds schematically. (b)–(d) The surface energy ratio $\gamma_{(001)}/\gamma_{(101)}$ and the ratio of $1/\cos\theta$ with the variation of the applied strain. The anatase (001) surface appears only when the surface energy ratio is smaller than $1/\cos\theta$.

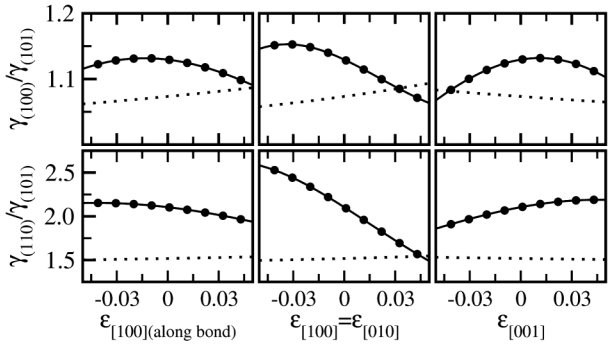

FIG. 4. Comparison of the surface energy normalized to $\gamma_{(101)}$ (solid curves) and the critical condition (dotted curves) of presentation of the two low-index surfaces (100) (a) and (110) (b). The surface appears only when the corresponding solid curve goes below the dotted curve.

In order to understand the different behaviors of the area ratio under different strain, we plot in Figs. 3(b)–3(d) the ratio of the (001) surface energy to the (101) surface energy as a function of the strain. Also shown is the variation of $1/\cos\theta$. According to the rule of Wulff construction, the area percentage of the (001) surface increases with θ and decreases with $\gamma_{(001)}/\gamma_{(101)}$. We can see that $1/\cos\theta$ increases and $\gamma_{(001)}/\gamma_{(101)}$ decreases, with increasing biaxial compressive strain along the a axes or uniaxial strain along the surface bonds. It suggests that the proportion of the (001) surface increases, which is consistent with that shown in Fig. 3(a). For strain along [001], the situation is contrary to that.

Up to now we are under the assumption that only {001} and {101} surfaces present in the equilibrium shape of anatase, even under strain. In order to verify the assumption, we need to consider the condition for the other low-index surfaces to appear in anatase. For instance, $\frac{\gamma_{(100)}}{\gamma_{(101)}} \leq \frac{1}{\sin\theta}$ and $\frac{\gamma_{(110)}}{\gamma_{(101)}} \leq \frac{\sqrt{2}}{\sin\theta}$ for (100) and (110) to be present, respectively. In Fig. 4, we plot the variation of the surface energy ratio as well as the critical values for the surfaces to appear. It shows that the (100) and (110) surfaces do not appear under all the strain when the area percentage of the (001) surface increases.

External strain is usually applied by using the lattice mismatch between the substrate and the crystal [29]. A modification of the Wulff construction, called the Winterbottom construction, is used to predict the equilibrium shape of the crystal on a substrate. The Wulff shape is truncated at a plane in parallel to the substrate, the location of which is determined by the difference between the interfacial free energy γ_i and the substrate free energy γ_s [30]. For the epitaxial growth of the (001) surface, the Wulff construction in this Letter corresponds to the Winterbottom construction when $\gamma_i - \gamma_s$ is equal to or larger than γ_{001} (nonwetting). The conclusion that the in-plane compressive strain increases the area percentage of the (001) surface still applies for the wetting situation that $\gamma_i - \gamma_s < \gamma_{001}$. Therefore, by selecting a suitable substrate, it is possible to synthesize single crystal anatase islands with a large percentage of the highly reactive (001) surface.

In summary, based on the density functional theory calculations, the bulk and surface elastic properties of rutile and anatase TiO_2 are calculated. The influence of the applied strain on the surface energies and hence the area ratio of anatase crystallite is investigated. We find that when ~5% compressive strain is applied biaxially along the a axes, the area percentage of the most reactive anatase (001) surface can be increased by ~5 times in comparison with the crystallite without strain. If external strain is only applied during the growth process, the lattice parameters should relax back toward the equilibrium values once the external constraints are released. In this way, the surface reactivity is almost kept unchanged, so that the efficiency of surface reactivity can be increased as a result of increasing area proportion of the reactive (001) surface. Experimentally, the range of applied strain is limited to be moderate so that dislocation due to relaxation of strain is not significant. Since external strain can be easily applied by selecting specific substrate in epitaxial growth, we propose that it is a generic way to apply external strain to engineer the surface morphologies and control the surface reactivity.

The authors acknowledge helpful discussions with Dr. Suhuai Wei. The numerical calculations have been carried out at the High Performance Computing Center of Nanjing University and the Shanghai Supercomputer Center. This work was supported by MOST of China (under Grants No. 2010CB630705 and No. 2012CB921502), NSF of China (under Grants No. 10974079, No. 11174123, No. 11034005, and No. 50972057), and MOE of China (under Grant No. NCET-09-0461).

*djshu@nju.edu.cn
†muwang@nju.edu.cn

[1] R. Asahi, T. Morikawa, T. Ohwaki, K. Aoki, and Y. Taga, Science **293**, 269 (2001).
[2] C. T. Campbell, S. C. Parker, and D. E. Starr, Science **298**, 811 (2002).
[3] M. Gratzel, Nature (London) **414**, 338 (2001).
[4] O. Bikondoa, C. L. Pang, R. Ithnin, C. A. Muryn, H. Onishi, and G. Thornton, Nature Mater. **5**, 189 (2006).
[5] G. Lu, A. Linsebigler, and J. T. Yates, J. Phys. Chem. **99**, 7626 (1995).
[6] A. Vittadini, M. Casarin, and A. Selloni, Theor. Chem. Acc. **117**, 663 (2007).
[7] M. Lazzeri, A. Vittadini, and A. Selloni, Phys. Rev. B **63**, 155 409 (2001).
[8] U. Diebold, N. Ruzycki, G. S. Herman, and A. Selloni, Catal. Today **85**, 93 (2003).

[9] A. Zangwill, *Physics at Surfaces* (Cambridge University Press, Cambridge, England, 1998).
[10] H. G. Yang, C. H. Sun, S. Z. Qiao, J. Zou, G. Liu, S. C. Smith, H. M. Cheng, and G. Q. Lu, Nature (London) **453**, 638 (2008).
[11] A. Selloni, Nature Mater. **7**, 613 (2008).
[12] C. Z. Wen, H. B. Jiang, S. Z. Qiao, H. G. Yang, and G. Q. Lu, J. Mater. Chem. **21**, 7052 (2011).
[13] L. Thulin and J. Guerra, Phys. Rev. B **77**, 195 112 (2008).
[14] W. J. Yin, S. Y. Chen, J. H. Yang, X. G. Gong, Y. F. Yan, and S. H. Wei, Appl. Phys. Lett. **96**, 221 901 (2010).
[15] D. J. Shu, S. T. Ge, M. Wang, and N. B. Ming, Phys. Rev. Lett. **101**, 116 102 (2008).
[16] Z. W. Wang, D. J. Shu, M. Wang, and N. B. Ming, Phys. Rev. B **82**, 165 309 (2010).
[17] R. E. Miller and V. B. Shenoy, Nanotechnology **11**, 139 (2000).
[18] J. P. Perdew, K. Burke, and M. Ernzerhof, Phys. Rev. Lett. **77**, 3865 (1996).
[19] G. Kresse and D. Joubert, Phys. Rev. B **59**, 1758 (1999).
[20] P. E. Blöchl, Phys. Rev. B **50**, 17 953 (1994).
[21] D. G. Isaak, J. D. Carnes, O. L. Anderson, H. Cynn, and E. Hake, Phys. Chem. Miner. **26**, 31 (1998).
[22] E. Shojaee and M. R. Mohammadizadeh, J. Phys. Condens. Matter **22**, 015401 (2010).
[23] H. Sato, K. Ono, T. Sasaki, and A. Yamagishi, J. Phys. Chem. B **107**, 9824 (2003).
[24] L. D. Landau and E. Lifshitz, *Theory of Elasticity* (Butterworth-Heinemann, Oxford, 1986), 3rd ed.
[25] H. Perron, C. Domain, J. Roques, R. Drot, E. Simoni, and H. Catalette, Theor. Chem. Acc. **117**, 565 (2007).
[26] V. B. Shenoy, Phys. Rev. B **71**, 094 104 (2005).
[27] M. Schmid, W. Hofer, P. Varga, P. Stoltze, K. W. Jacobsen, and J. K. Norskov, Phys. Rev. B **51**, 10 937 (1995).
[28] M. Lazzeri and A. Selloni, Phys. Rev. Lett. **87**, 266 105 (2001).
[29] M. S. J. Marshall and M. R. Castell, Phys. Rev. Lett. **102**, 146 102 (2009).
[30] W. L. Winterbottom, Acta Metall. **15**, 303 (1967).